Supporting Information for:

Complexation of halide ions to tyrosine: role of non-covalent interactions evidenced by IRMPD spectroscopy

Davide Corinti,[a] Barbara Gregori,[a] Leonardo Guidoni,[b] Debora Scuderi,[c] Terry McMahon,[d] Barbara Chiavarino,[a] Simonetta Fornarini,[a] Maria Elisa Crestoni[a,*]

Corresponding author:
*Tel: +39 06 4991 3596. Fax: +39 06 4991 3602.
Email: mariaelisa.crestoni@uniroma1.it

Contents :

Fig. S8 Optimized minimum energy structures for selected isomers (**TI_phe1**, **TI_pla1**, **TI_ter1**, **TI_ter2**, **TI_zw1**, and **TI_zw2**) of $[Tyr+I]^-$. Relative enthalpies and relative free energies (bracketed) at the B3LYP/6-311++G(d,p) (in red), B3LYP-D3/6-311++G(d,p) (in blue) and MP2//B3LYP/6-311++G(d,p) (in black) levels are provided at 298 K in kJ mol^{-1}.

Fig. S9 Optimized minimum energy structures for selected isomers (**nTCl_ter2**, **nTCl_ter3**, **nTCl_pla3**, **nTCl_ter4**, **nTCl_zw2**, **nTCl_ring2**, **nTCl_O1**) of $[nitroTyr+Cl]^-$. Relative enthalpies and relative free energies (bracketed) at the B3LYP/6-311++G(d,p) (in red), B3LYP-D3/6-311++G(d,p) (in blue) and MP2//B3LYP/6-311++G(d,p) (in black) levels are provided at 298 K in kJ mol^{-1}. Thermodynamic data are relative to the calculated energies of the most stable isomer presented in Fig. 3 (**nTCl_pla1**).

Fig. S10 Optimized geometry deriving from an initial structure whereby HCl is acting as hydrogen bond donor towards both phenoxide oxygen and an oxygen atom of the nitro group. This species (**ST-1**) is not a minimum being characterized by an imaginary frequency. Relative enthalpies and relative free energies (bracketed) at the B3LYP/6-311++G(d,p) (in red), and B3LYP-D3/6-311++G(d,p) (in blue) levels are provided at 298 K in kJ mol^{-1}.

Fig. S11 Optimized minimum energy structures for selected isomers (**nTBr_pla1**, **nTBr_ter1**, **nTBr_pla2**, **nTBr_ring1**, **nTBr_ter2**, **nTBr_phe1**, **nTBr_zw1**, **nTBr_zw2**) of $[nitroTyr+Br]^-$. Relative enthalpies and relative free energies (bracketed) at the B3LYP/6-311++G(d,p) (in red), B3LYP-D3/6-311++G(d,p) (in blue) and MP2//B3LYP/6-311++G(d,p) (in black) levels are provided at 298 K in kJ mol^{-1}.

Fig. S12 Optimized minimum energy structures for selected isomers (**nTI_pla1**, **nTI_ter1**, **nTI_pla2**, **nTI_ring1**, **nTI_ter2**, **nTI_phe1**, **nTI_zw1**, **nTI_zw2**) of $[nitroTyr+I]^-$. Relative enthalpies and relative free energies (bracketed) at the B3LYP/6-311++G(d,p) (in red), B3LYP-D3/6-311++G(d,p) (in blue) and MP2//B3LYP/6-311++G(d,p) (in black) levels are provided at 298 K in kJ mol^{-1}.

Fig. S13 Experimental IRMPD spectra of $[Tyr+Cl]^-$ (green profile) and $[Tyr+Br]^-$ (brown profile) in the NH/OH stretch range compared with IR spectra [km mol^{-1}] for **TCl_pla1**, **TCl_phe1**, **TCl_ter1**, **TCl_ter2**, **TCl_zw1** and **TBr_phe1**, **TBr_pla1**, **TBr_ter1**, **TBr_ter2**, **TBr_zw1** structures obtained at the B3LYP/6-311++G(d,p) level of theory and scaled by a factor of 0.955. The pale profiles report the experimental $[Tyr+Cl]^-$ (pale green) and $[Tyr+Br]^-$ (pale brown) spectra.

Fig. S14 Experimental IRMPD spectra of: $[Tyr+Cl]^-$ (green profile, panel A) compared with IR spectra [km mol^{-1}] for **TCl_phe2**, **TCl_pla2**, **TCl_phe3**, **TCl_zw2** structures; $[Tyr+Br]^-$ (brown profile, panel B) compared with IR spectra [km mol^{-1}] for **TBr_zw2**; $[Tyr+I]^-$ (purple profile, panel C) compared with IR spectra [km mol^{-1}] for **TI_zw2**. Theoretical vibrational modes were obtained at the B3LYP/6-311++G(d,p) level of theory and scaled by a factor of 0.978.

Fig. S15 Averaged spectrum of $[Tyr+Cl]^-$ computed from the calculated Boltzmann populations of **TCl_pla1**, **TCl_phe1** and **TCl_ter1** obtained from single-point free energy calculations at MP2//B3LYP/6-311++G(d,p) level. The experimental spectrum (green profile) is also shown to enable comparison.

Fig. S16 Experimental IRMPD spectrum (green profile) of chloride-bound 3-NO_2-tyrosine adduct, $[nitroTyr+Cl]^-$, compared with IR spectra [km mol^{-1}] for **nTCl_pla2**, **nTCl_ter2**, **nTCl_ter3**, **nTCl_pla3**, **nTCl_ter4**, **nTCl_zw2**, **nTCl_ring2**, **nTCl_O1** structures obtained at the B3LYP/6-311++G(d,p) level of theory and scaled by a factor of 0.978.

Fig. S17 Experimental IRMPD spectra of: $[nitroTyr+Br]^-$ (brown profile, panel A) compared with IR spectra [km mol^{-1}] for **nTBr_pla1**, **nTBr_ter1**, **nTBr_ring1** and **nTBr_ter2** structures; $[nitroTyr+I]^-$ (purple profile, panel B) compared with IR spectra [km mol^{-1}] for **nTI_pla1**, **nTI_ter1**, **nTI_ring1** and **nTI_ter2** structures. Theoretical vibrational modes were obtained at the B3LYP/6-311++G(d,p) level of theory and scaled by a factor of 0.978. Relative enthalpies and relative free energies (bracketed) at the B3LYP/6-311++G(d,p) (in red), B3LYP-D3/6-311++G(d,p) (in blue) and MP2//B3LYP/6-311++G(d,p) (in black) levels are provided at 298 K in kJ mol^{-1}.

Fig. S18 Experimental IRMPD spectra of: $[nitroTyr+Br]^-$ (brown profile, panel A) compared with IR spectra [km mol^{-1}] for **nTBr_pla2**, **nTBr_phe1**, **nTBr_zw1** and **nTBr_zw2** structures; $[nitroTyr+I]^-$ (purple profile, panel B) compared with IR spectra [km mol^{-1}] for **nTI_pla2**, **nTI_phe1**, **nTI_zw1** and **nTI_zw2** structures. Theoretical vibrational modes were obtained at the B3LYP/6-311++G(d,p) level of theory and scaled by a factor of 0.978.

Table S1 Calculated energies (kJ mol^{-1}) at the B3LYP/6-311++G** level for the reaction: $[(nitro)Tyr+X]^- \rightarrow (nitro)Tyr + X^-$ (X = Cl, Br, I).

Table S2 Thermodynamic data (kJ mol^{-1}) for the most stable structures of $[Tyr+X]^-$ (X = Cl, Br, I) adducts calculated at different levels of theory.

TABLE S3 Selected dihedral angles (in Degrees) of the lowest energy structures of $[Tyr+X]^-$ (X = Cl, Br, I) adducts, calculated at the B3LYP/6-311++G(d,p) level of theory.

Table S4 Thermodynamic data (kJ mol^{-1}) for the most stable structures of $[nitroTyr+X]^-$ (X = Cl, Br, I) adducts calculated at different levels of theory.

TABLE S5 Selected dihedral angles (in Degrees) of the lowest energy structures of $[nitroTyr+X]^-$ (X = Cl, Br, I) adducts, calculated at the B3LYP/6-311++G(d,p) level of theory.

Table S6 Experimental IRMPD resonances and calculated (at B3LYP/6-311++G(d,p) level of theory) vibrational frequencies for the low-lying isomers of $[Tyr+X]^-$ (X = Cl, Br, I) adducts.

Table S7 Experimental IRMPD resonances and calculated (at B3LYP/6-311++G(d,p) level of theory) vibrational frequencies for the low-lying isomers of $[nitroTyr+X]^-$ (X = Cl, Br, I) adducts.

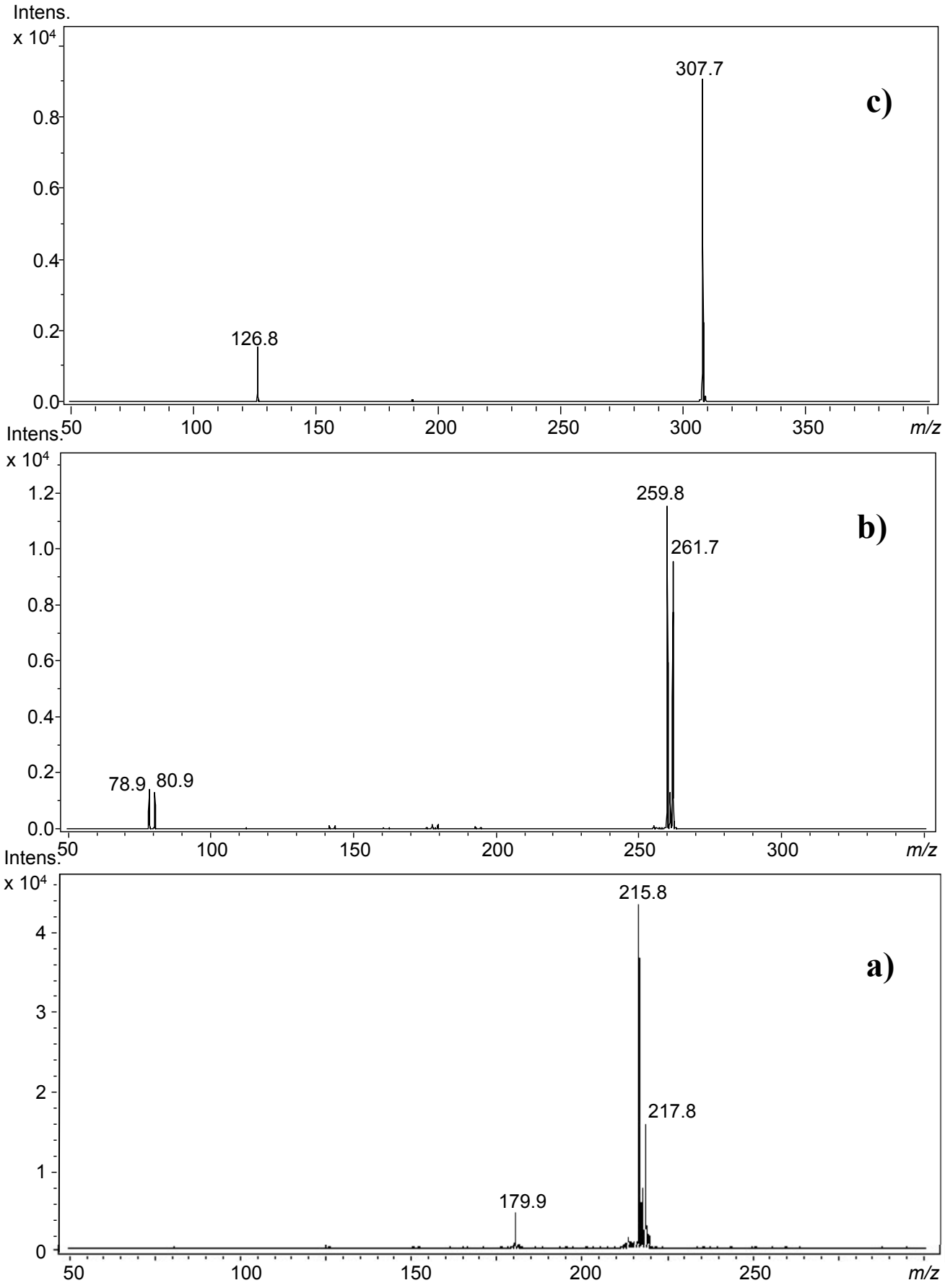

Fig. S1 Negative ESI mass spectra recorded upon selection of halide L-tyrosine adducts, a) $[Tyr+Cl]^-$ (*m/z* 216/218); b) $[Tyr+Br]^-$ (*m/z* 260/262); and c) $[Tyr+I]^-$ (*m/z* 308), upon irradiation with CLIO FEL light on resonance at 1505, 1297, 1177 cm^{-1}, respectively. Spectra recorded in a Bruker Esquire Paul ion trap mass spectrometer (Bruker, Esquire 3000+).

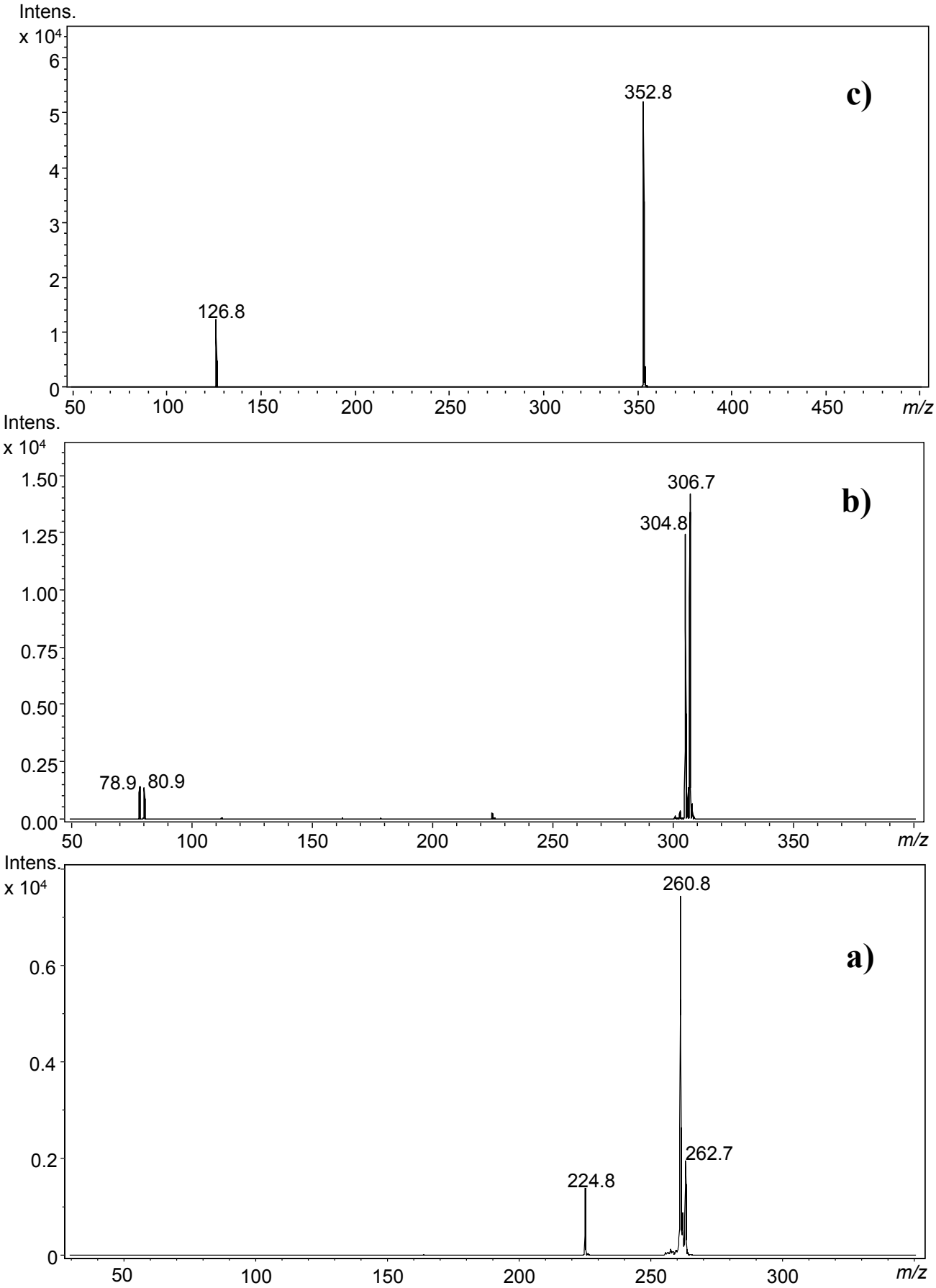

Fig. S2 Negative ESI mass spectra recorded upon selection of halide 3-NO_2-L-tyrosine adducts, a) $[nitroTyr+Cl]^-$ (*m/z* 261/263); b) $[nitroTyr+Br]^-$ (*m/z* 305/307); and c) $[nitroTyr+I]^-$ (*m/z* 353), upon irradiation with CLIO FEL light on resonance at 1477, 1325, 1737 cm^{-1}, respectively. Spectra recorded in a Bruker Esquire Paul ion trap mass spectrometer (Bruker, Esquire 3000+).

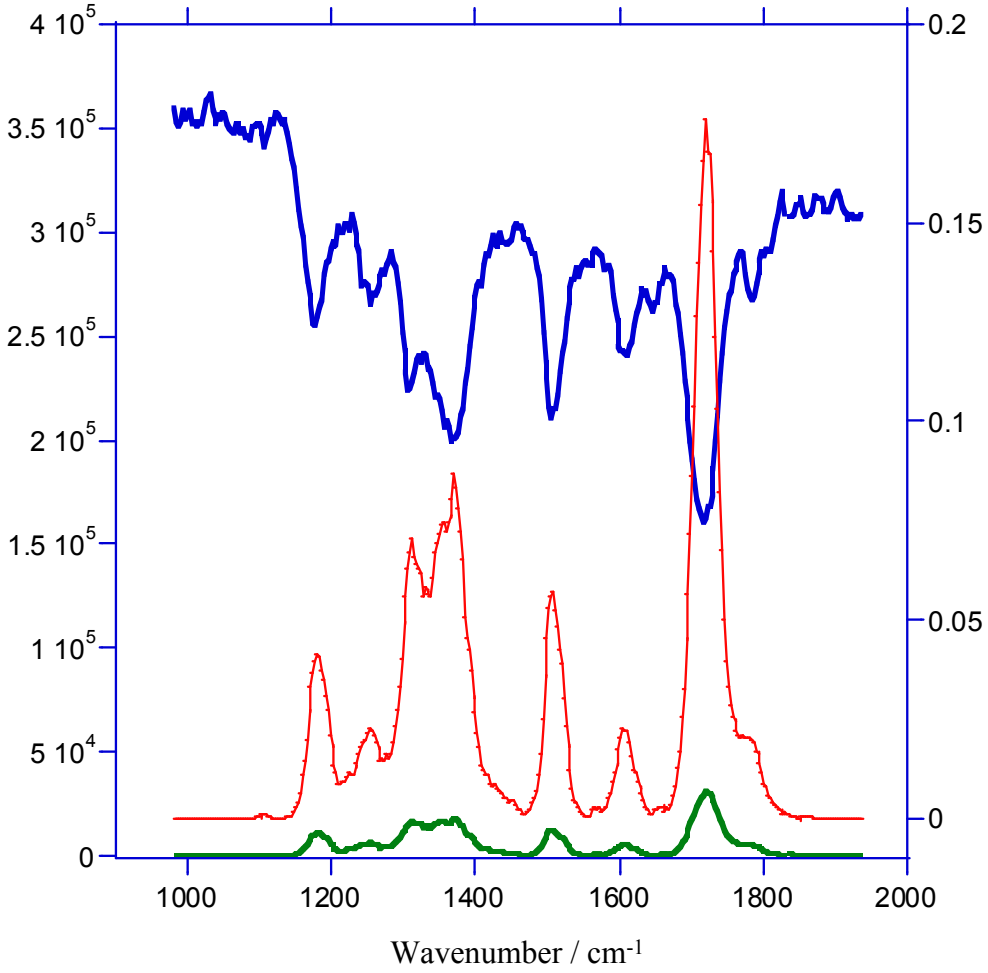

Fig. S3 Experimental IRMPD signals of $[Tyr+Cl]^-$ recorded in the parent ion channel depletion ($[Tyr+Cl]^-$, blue profile), the fragment ion channel ($[Tyr-H]^-$, green profile), and the IRMPD efficiency (*R*, red profile) in the 950-1950 cm^{-1} range. R scale is on the right vertical axis and ion abundances (in arbitrary units) are on the left vertical axis.

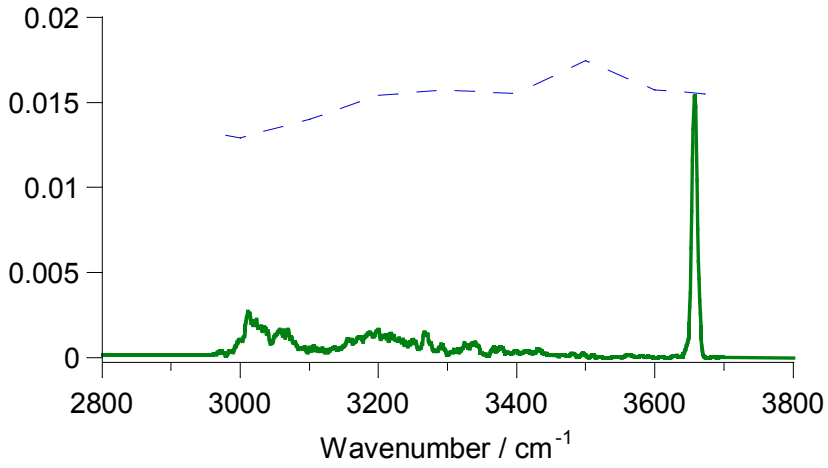

Fig. S4 Experimental IRMPD spectrum of $[Tyr+Cl]^-$ (green profile) in the 2800-3800 cm^{-1} range. The blue dashed profile shows the laser power as a function of the IR wavenumber.

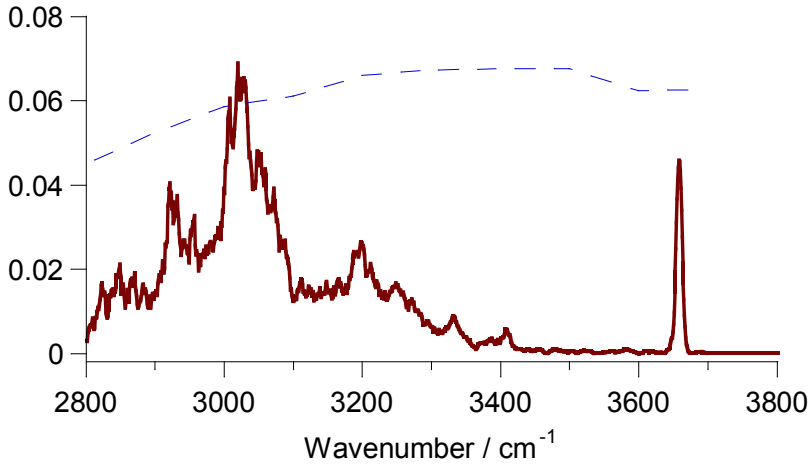

Fig. S5 Experimental IRMPD spectrum of $[Tyr+Br]^-$ (brown profile) in the 2800-3800 cm^{-1} range. The blue dashed profile shows the laser power as a function of the IR wavenumber.

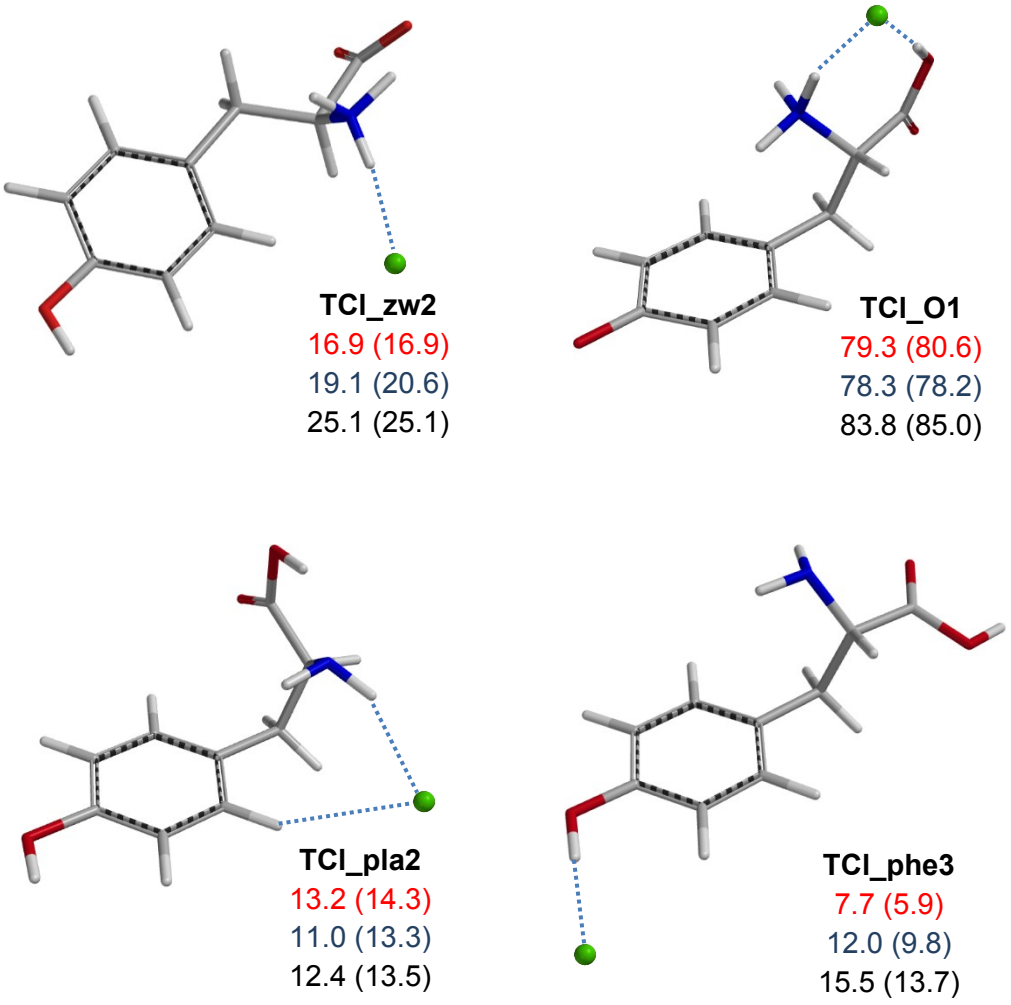

Fig. S6 Optimized minimum energy structures for selected isomers (**TCl_pla2**, **TCl_phe3**, **TCl_zw2**, and **TCl_O1**) of [Tyr+Cl]$^-$. Relative enthalpies and relative free energies (bracketed) at the B3LYP/6-311++G(d,p) (in red), B3LYP-D3/6-311++G(d,p) (in blue) and MP2//B3LYP/6-311++G(d,p) (in black) levels are provided at 298 K in kJ mol^{-1}. Thermodynamic data are relative to the calculated energies of the most stable isomer presented in Fig. 2 (**TCl_pla1**).

The monodentate **TCl_phe3**, 13.7 5 kJ mol^{-1} above the global minimum, features chloride coordinated to the phenol site, and a *right*, *gauche* structure, which arises from the rotation about the C1-C2 and O1-C1 bonds of **TCl_phe1**. These changes modify the ∠O1C1C2N dihedral angle to 150.7° for **TCl_phe3** and allows the amino hydrogen to interact with the carbonyl oxygen ($r_{CO...HN}$ = 2.48 Å) of the carboxylic acid in a *cis* arrangement. The bidentate **TCl_pla2** structure, 13.5 kJ mol^{-1} above the global minimum is endowed with a *left*, *gauche* geometry, obtained by rotation of C1C2, C2C3, and C2N bonds of **TCl_pla1**, and binds chloride between amine ($r_{Cl...HN}$ = 2.28 Å) and aromatic ($r_{Cl...HC}$ = 2.89 Å) hydrogens, while the carboxylic acid in *trans* interacts as a H-bond donor with the N-terminus ($r_{N...HOC}$ = 1.81 Å). Not unexpectedly, from the above comparison it turns out that the dual CH···Cl···HOC(O) hydrogen-bonding interactions (in **TCl_pla1**) are more beneficial than CH···Cl···HN (in **TCl_pla2**) in stabilizing chloride-bound tyrosine adduct.

The **TCl_zw2** conformer, with a more extended conformation than **TCl_zw1** results 25.1 kJ mol^{-1} less favorable than **TCl_pla1**.

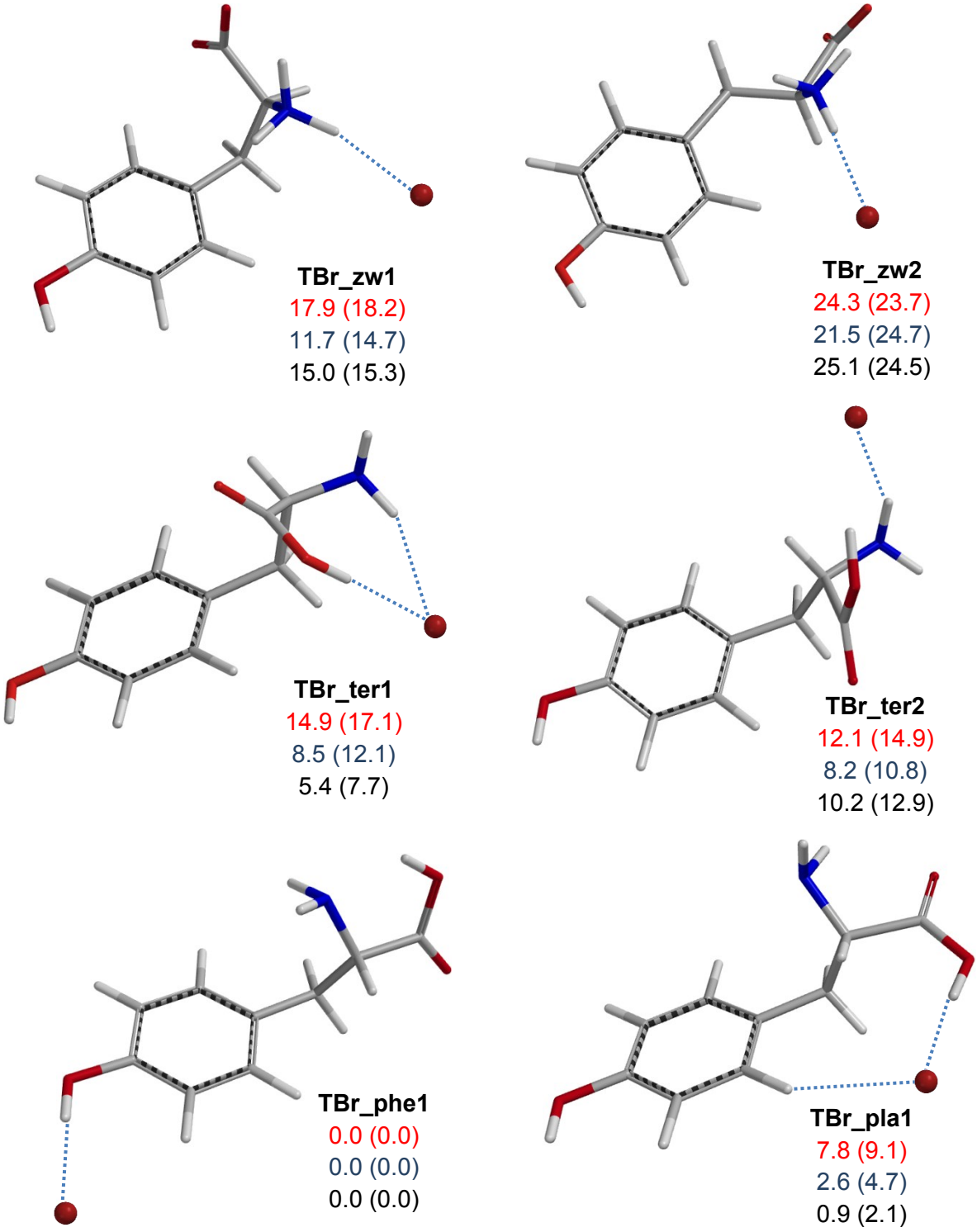

Fig. S7 Optimized minimum energy structures for selected isomers (**TBr_phe1**, **TBr_pla1**, **TBr_ter1, TBr_ter2**, **TBr_zw1**, and **TBr_zw2**) of $[Tyr+Br]^-$. Relative enthalpies and relative free energies (bracketed) at the B3LYP/6-311++G(d,p) (in red), B3LYP-D3/6-311++G(d,p) (in blue) and MP2//B3LYP/6-311++G(d,p) (in black) levels are provided at 298 K in kJ mol^{-1}.

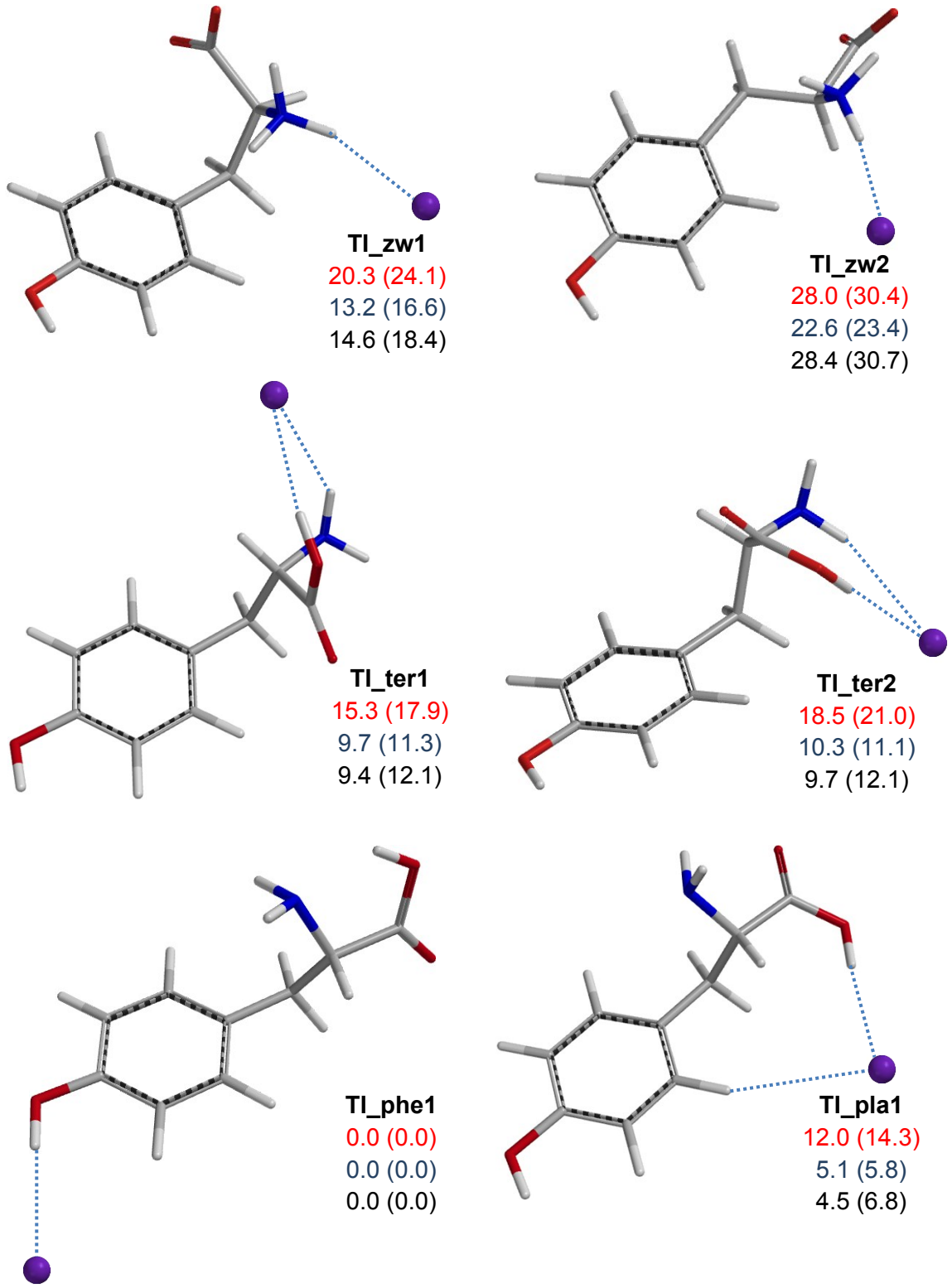

Fig. S8 Optimized minimum energy structures for selected isomers (**TI_phe1**, **TI_pla1**, **TI_ter1**, **TI_ter2**, **TI_zw1**, and **TI_zw2**) of $[Tyr+I]^-$. Relative enthalpies and relative free energies (bracketed) at the B3LYP/6-311++G(d,p) (in red), B3LYP-D3/6-311++G(d,p) (in blue) and MP2//B3LYP/6-311++G(d,p) (in black) levels are provided at 298 K in kJ mol^{-1}.

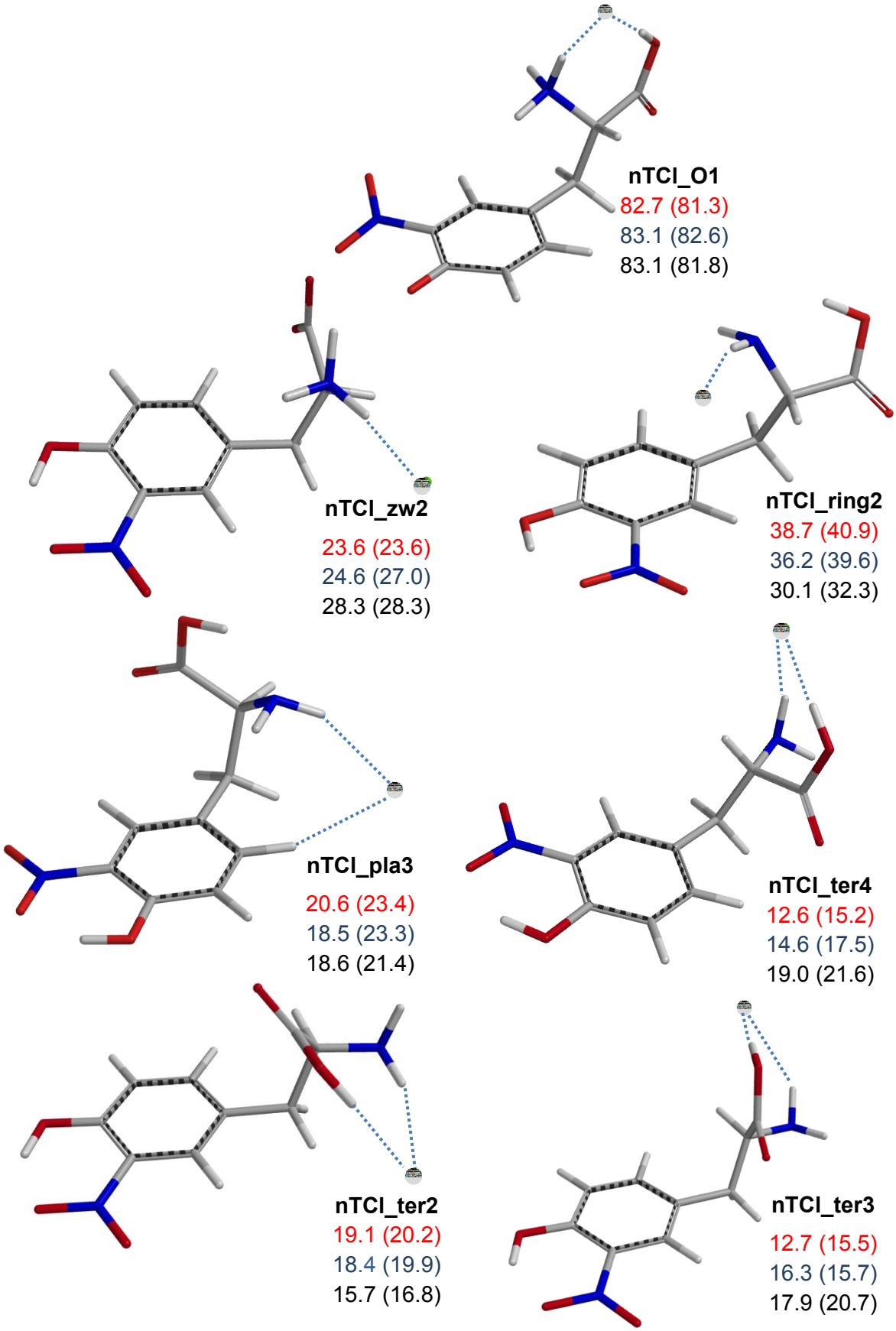

Fig. S9 Optimized minimum energy structures for selected isomers (**nTCl_ter2**, **nTCl_ter3**, **nTCl_pla3**, **nTCl_ter4**, **nTCl_zw2**, **nTCl_ring2**, **nTCl_O1**) of [nitroTyr+Cl]$^{-}$. Relative enthalpies and relative free energies (bracketed) at the B3LYP/6-311++G(d,p) (in red), B3LYP-D3/6-311++G(d,p) (in blue) and MP2//B3LYP/6-311++G(d,p) (in black) levels are provided at 298 K in kJ mol^{-1}. Thermodynamic data are relative to the calculated energies of the most stable isomer presented in Fig. 3 (**nTCl_pla1**).

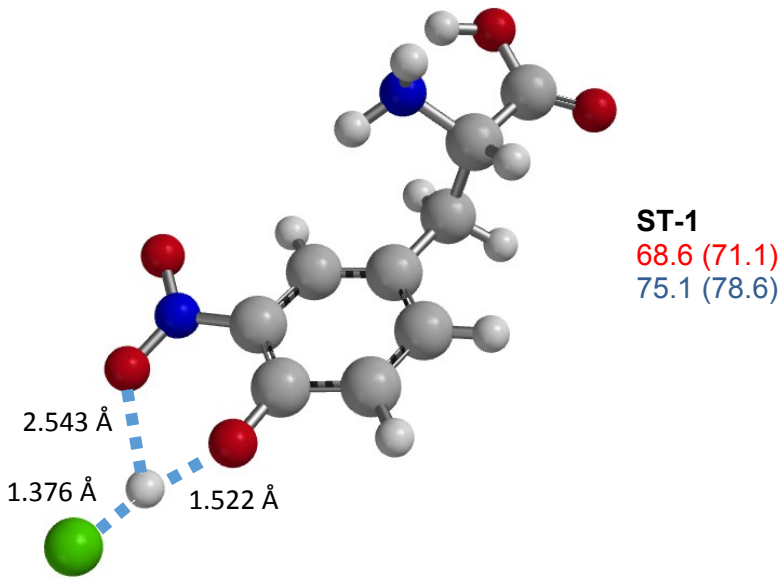

Fig. S10 Optimized geometry deriving from an initial structure whereby HCl is acting as hydrogen bond donor towards both phenoxide oxygen and an oxygen atom of the nitro group. This species (**ST-1**) is not a minimum being characterized by an imaginary frequency. Relative enthalpies and relative free energies (bracketed) at the B3LYP/6-311++G(d,p) (in red), and B3LYP-D3/6-311++G(d,p) (in blue) levels are provided at 298 K in kJ mol^{-1}. Interatomic bond distances, marked by dashed lines, are reported in Å.

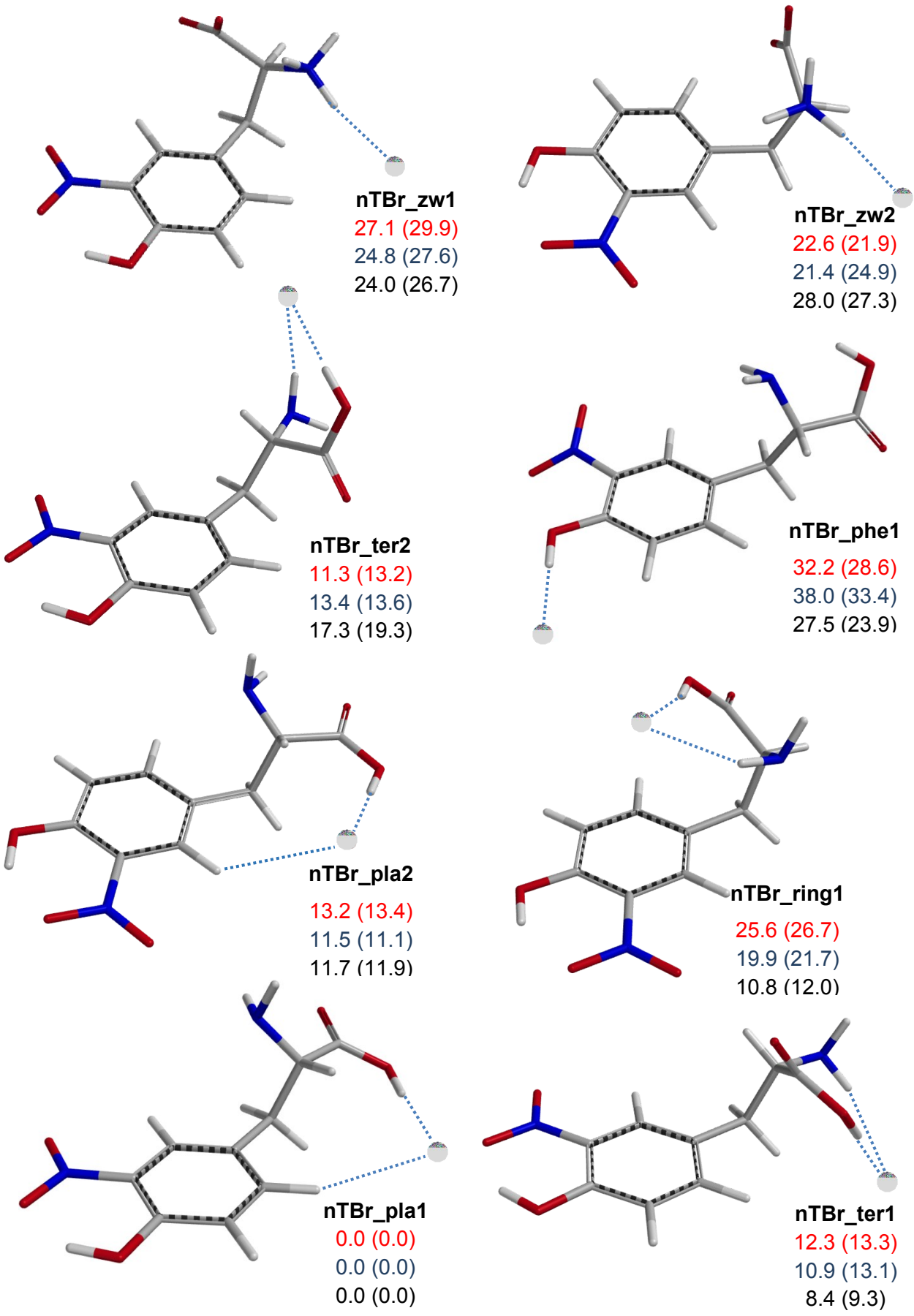

Fig. S11 Optimized minimum energy structures for selected isomers (**nTBr_pla1**, **nTBr_ter1**, **nTBr_pla2**, **nTBr_ring1**, **nTBr_ter2**, **nTBr_phe1**, **nTBr_zw1**, **nTBr_zw2**) of [nitroTyr+Br]$^-$. Relative enthalpies and relative free energies (bracketed) at the B3LYP/6-311++G(d,p) (in red), B3LYP-D3/6-311++G(d,p) (in blue) and MP2//B3LYP/6-311++G(d,p) (in black) levels are provided at 298 K in kJ mol^{-1}.

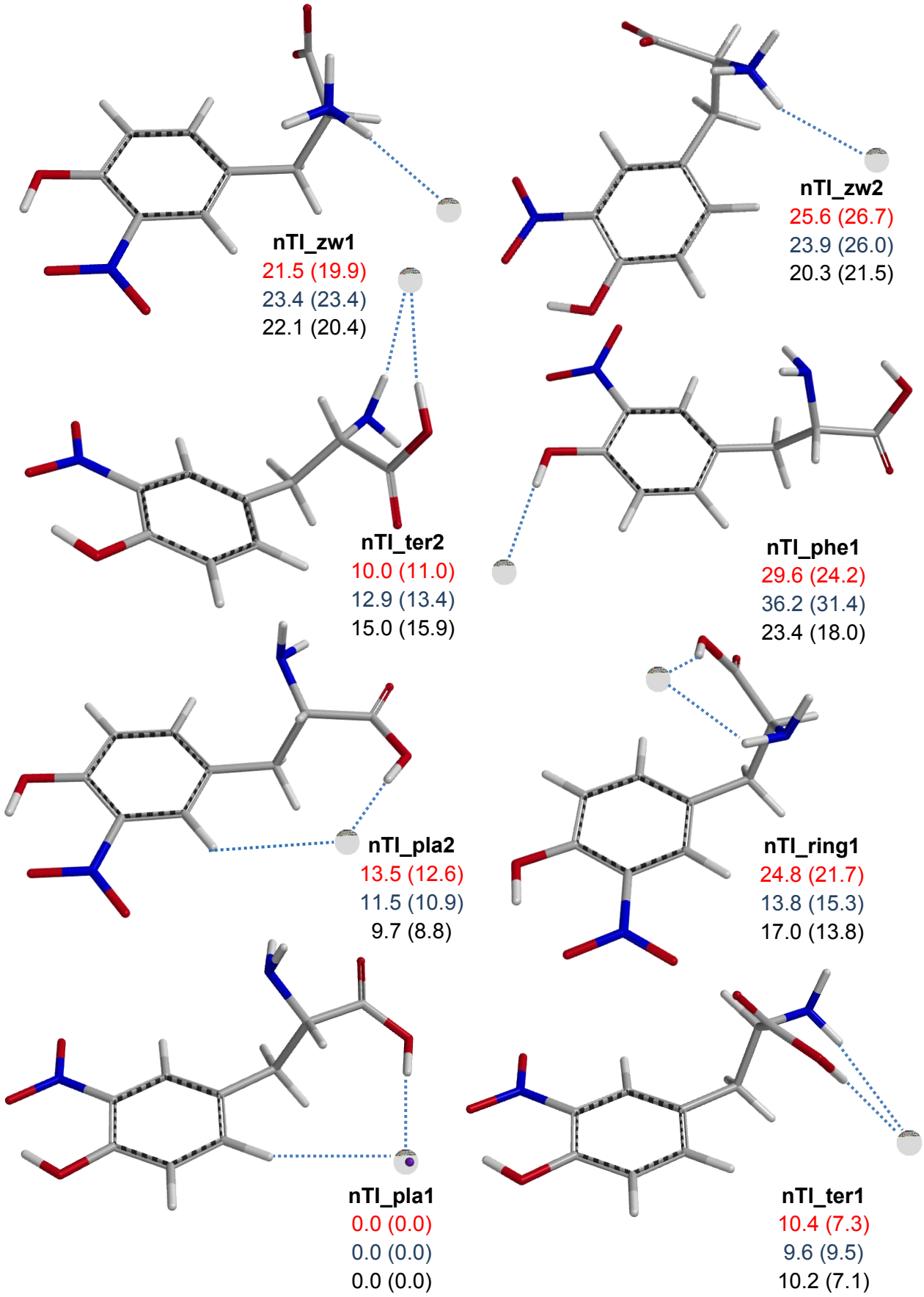

Fig. S12 Optimized minimum energy structures for selected isomers (**nTI_pla1**, **nTI_ter1**, **nTI_pla2**, **nTI_ring1**, **nTI_ter2**, **nTI_phe1**, **nTI_zw1**, **nTI_zw2**) of [nitroTyr+I]$^{-}$. Relative enthalpies and relative free energies (bracketed) at the B3LYP/6-311++G(d,p) (in red), B3LYP-D3/6-311++G(d,p) (in blue) and MP2//B3LYP/6-311++G(d,p) (in black) levels are provided at 298 K in kJ mol^{-1}.

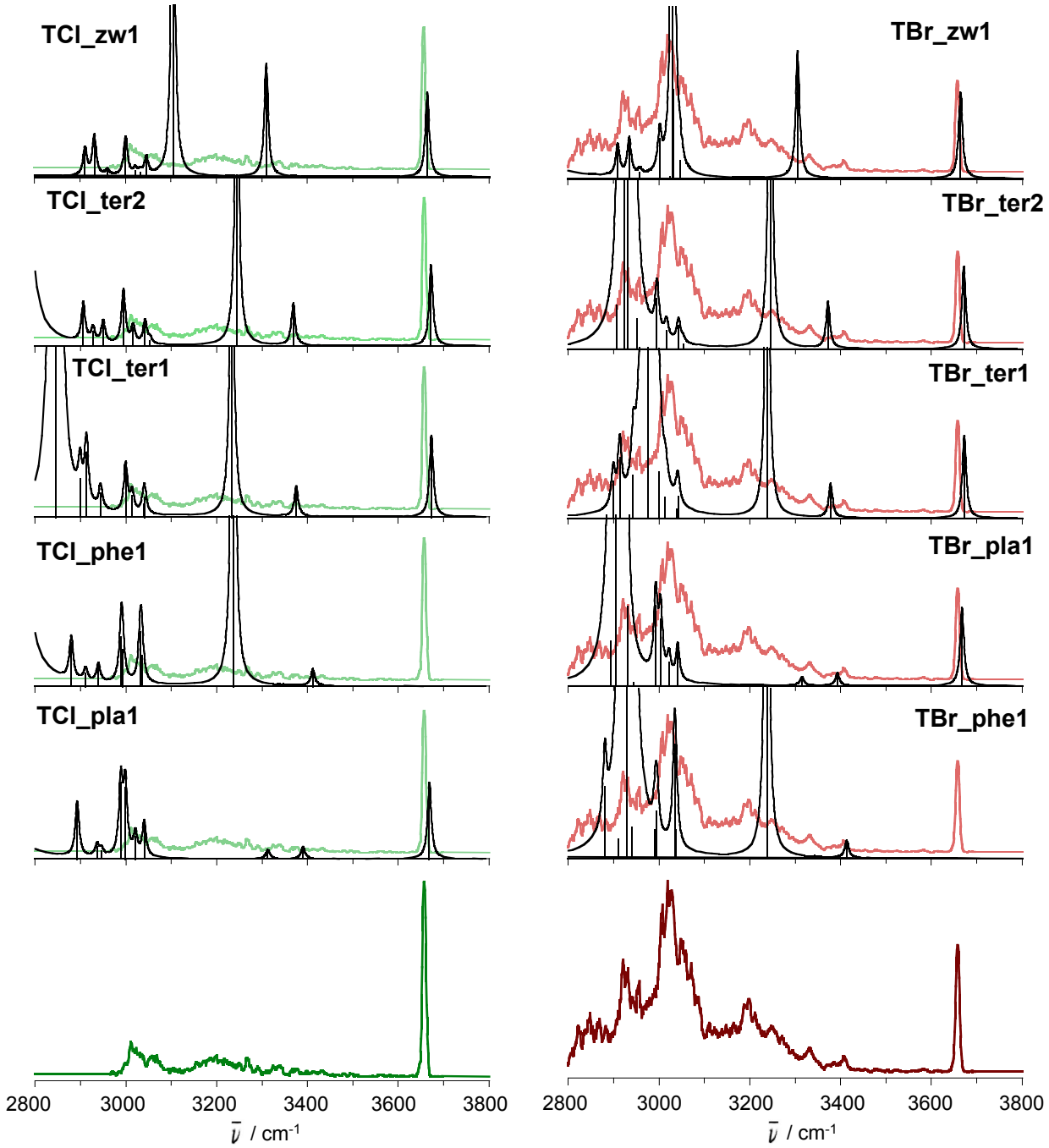

Fig. S13 Experimental IRMPD spectra of $[Tyr+Cl]^-$ (green profile) and $[Tyr+Br]^-$ (brown profile) in the NH/OH stretch range compared with IR spectra [km mol^{-1}] for **TCl_pla1**, **TCl_phe1**, **TCl_ter1**, **TCl_ter2**, **TCl_zw1** and **TBr_phe1**, **TBr_pla1**, **TBr_ter1**, **TBr_ter2**, **TBr_zw1** structures obtained at the B3LYP/6-311++G(d,p) level of theory and scaled by a factor of 0.955. The pale profiles report the experimental $[Tyr+Cl]^-$ (pale green) and $[Tyr+Br]^-$ (pale brown) spectra.

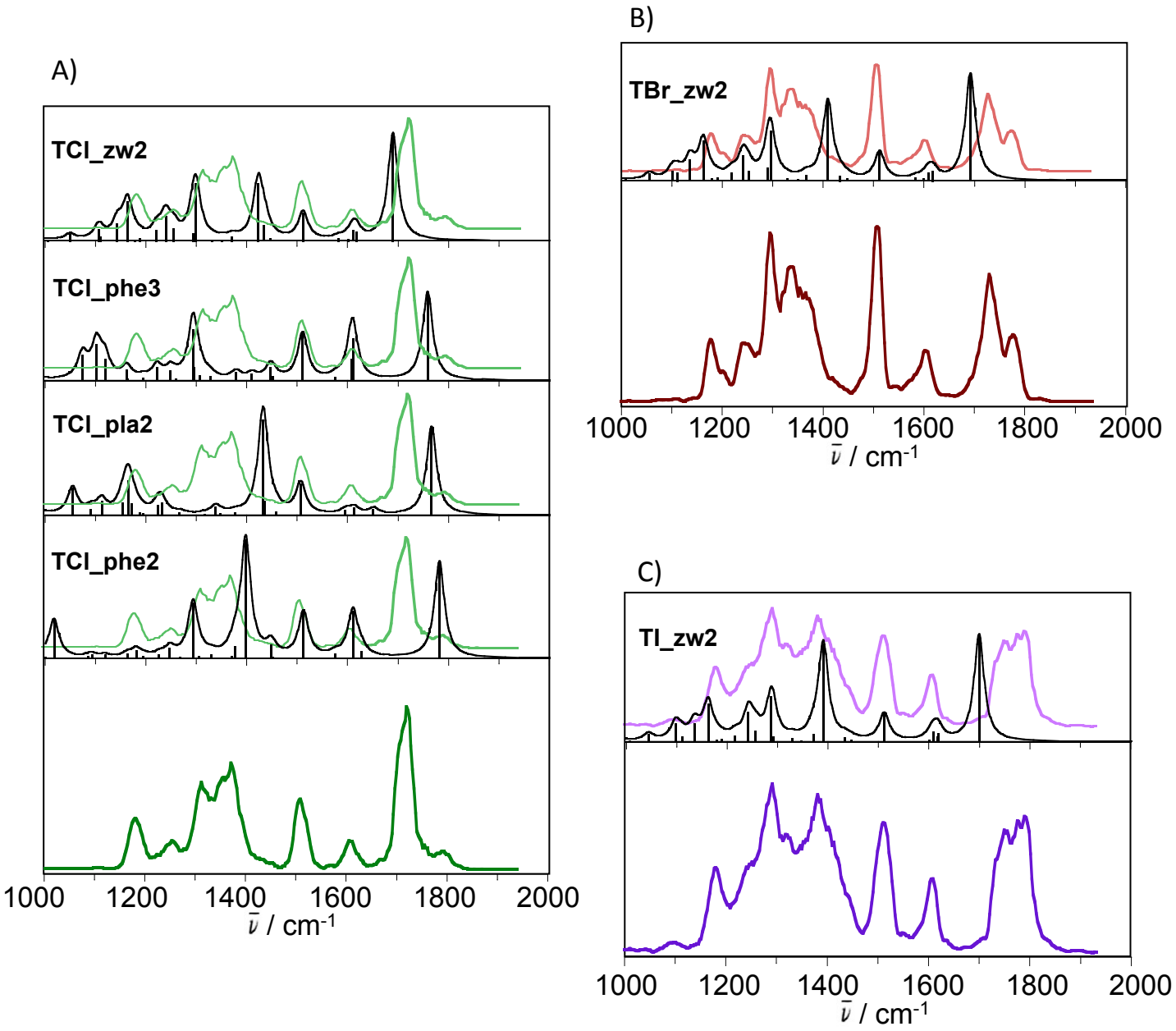

Fig. S14 Experimental IRMPD spectra of: $[Tyr+Cl]^-$ (green profile, panel A) compared with IR spectra [km mol^{-1}] for **TCl_phe2**, **TCl_pla2**, **TCl_phe3**, **TCl_zw2** structures; $[Tyr+Br]^-$ (brown profile, panel B) compared with IR spectra [km mol^{-1}] for **TBr_zw2**; $[Tyr+I]^-$ (purple profile, panel C) compared with IR spectra [km mol^{-1}] for **TI_zw2**. Theoretical vibrational modes were obtained at the B3LYP/6-311++G(d,p) level of theory and scaled by a factor of 0.978.

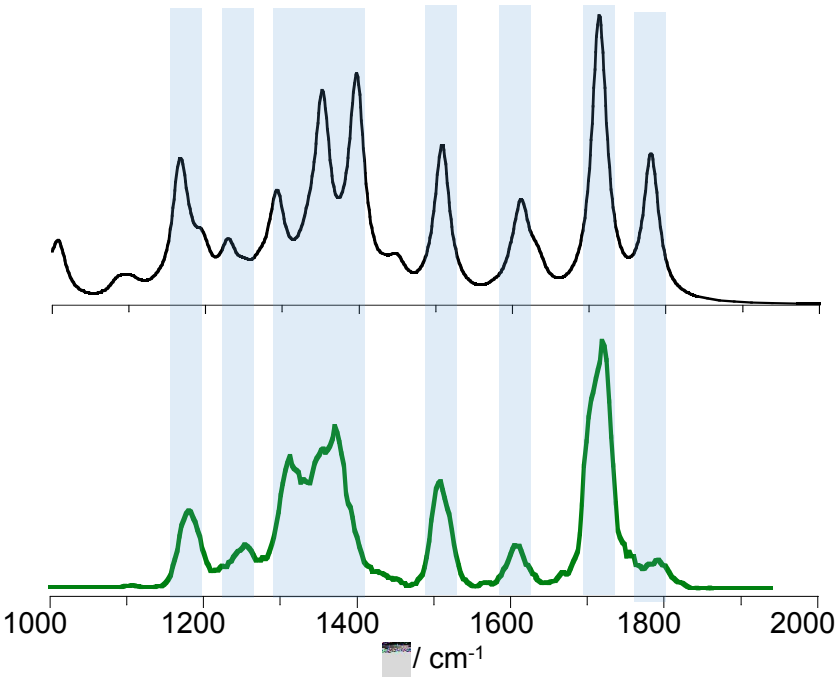

Fig. S15 Averaged spectrum of $[Tyr+Cl]^-$ computed from the calculated Boltzmann populations of **TCl_pla1**, **TCl_phe1** and **TCl_ter1** obtained from single-point free energy calculations at MP2//B3LYP/6-311++G(d,p) level. The experimental spectrum (green profile) is also shown to enable comparison.

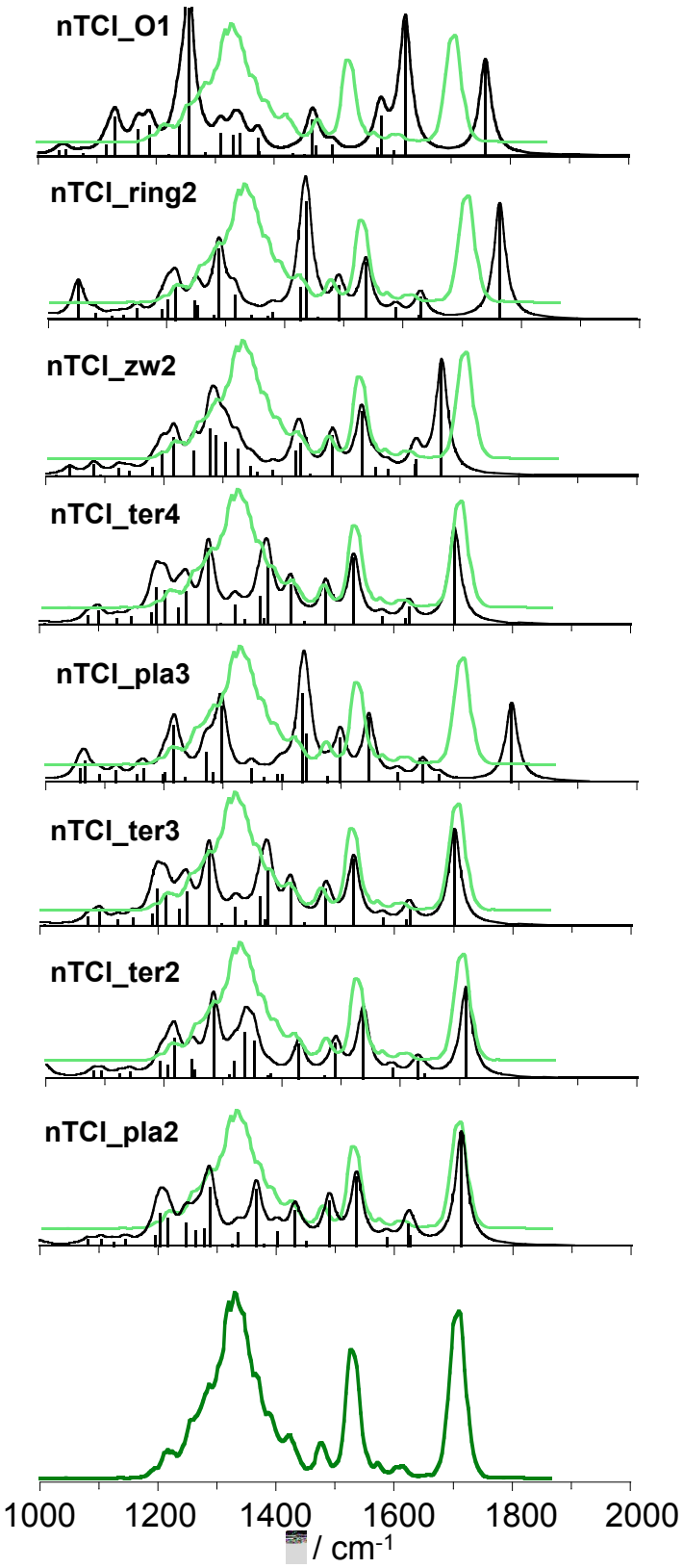

Fig. S16 Experimental IRMPD spectrum (green profile) of chloride-bound 3-NO_2-tyrosine adduct, $[nitroTyr+Cl]^-$, compared with IR spectra [km mol^{-1}] for **nTCl_pla2**, **nTCl_ter2**, **nTCl_ter3**, **nTCl_pla3**, **nTCl_ter4**, **nTCl_zw2**, **nTCl_ring2**, **nTCl_O1** structures obtained at the B3LYP/6-311++G(d,p) level of theory and scaled by a factor of 0.978.

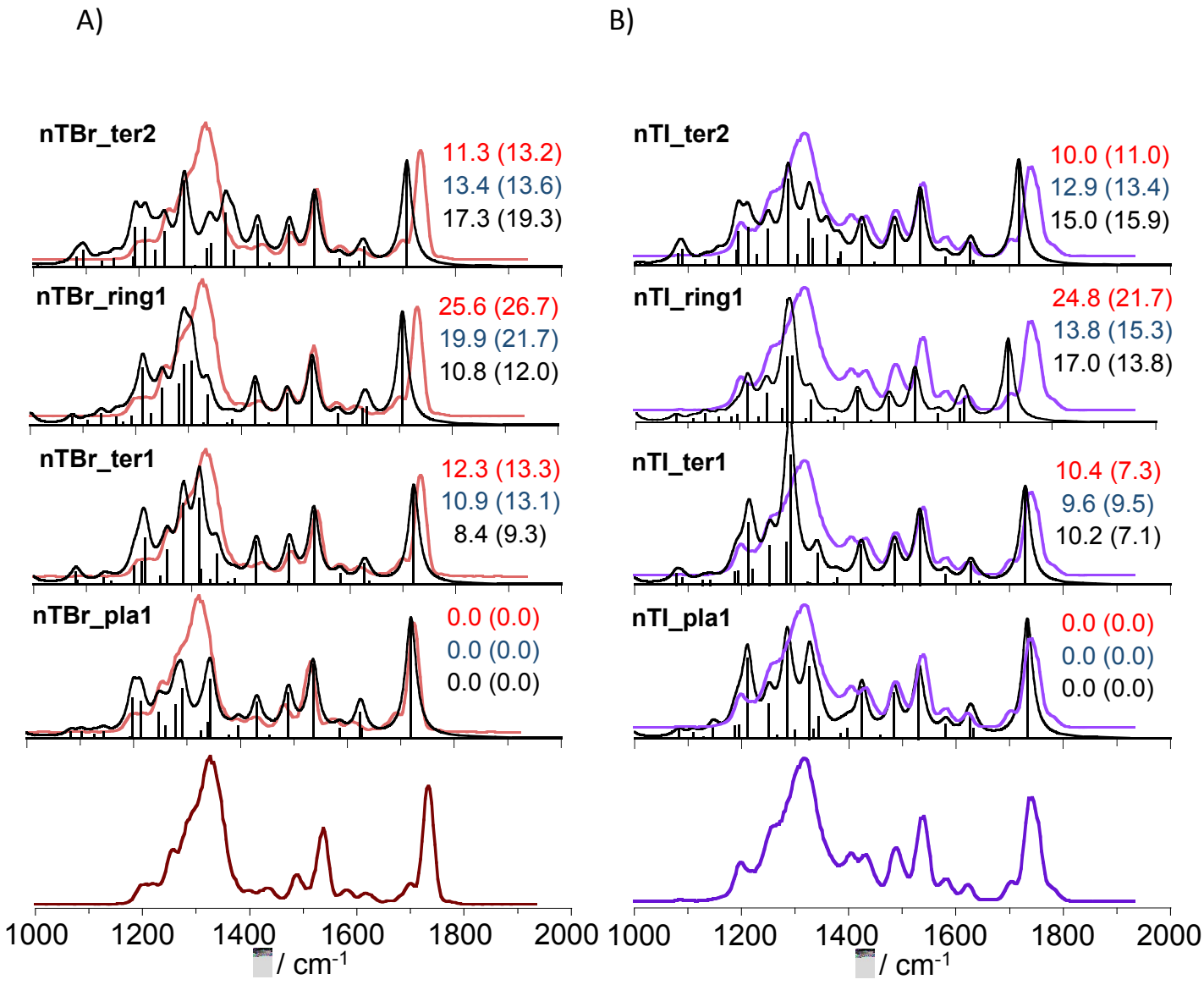

Fig. S17 Experimental IRMPD spectra of: $[nitroTyr+Br]^-$ (brown profile, panel A) compared with IR spectra [km mol^{-1}] for **nTBr_pla1**, **nTBr_ter1**, **nTBr_ring1** and **nTBr_ter2** structures; $[nitroTyr+I]^-$ (purple profile, panel B) compared with IR spectra [km mol^{-1}] for **nTI_pla1**, **nTI_ter1**, **nTI_ring1** and **nTI_ter2** structures. Theoretical vibrational modes were obtained at the B3LYP/6-311++G(d,p) level of theory and scaled by a factor of 0.978. Relative enthalpies and relative free energies (bracketed) at the B3LYP/6-311++G(d,p) (in red), B3LYP-D3/6-311++G(d,p) (in blue) and MP2//B3LYP/6-311++G(d,p) (in black) levels are provided at 298 K in kJ mol^{-1}.

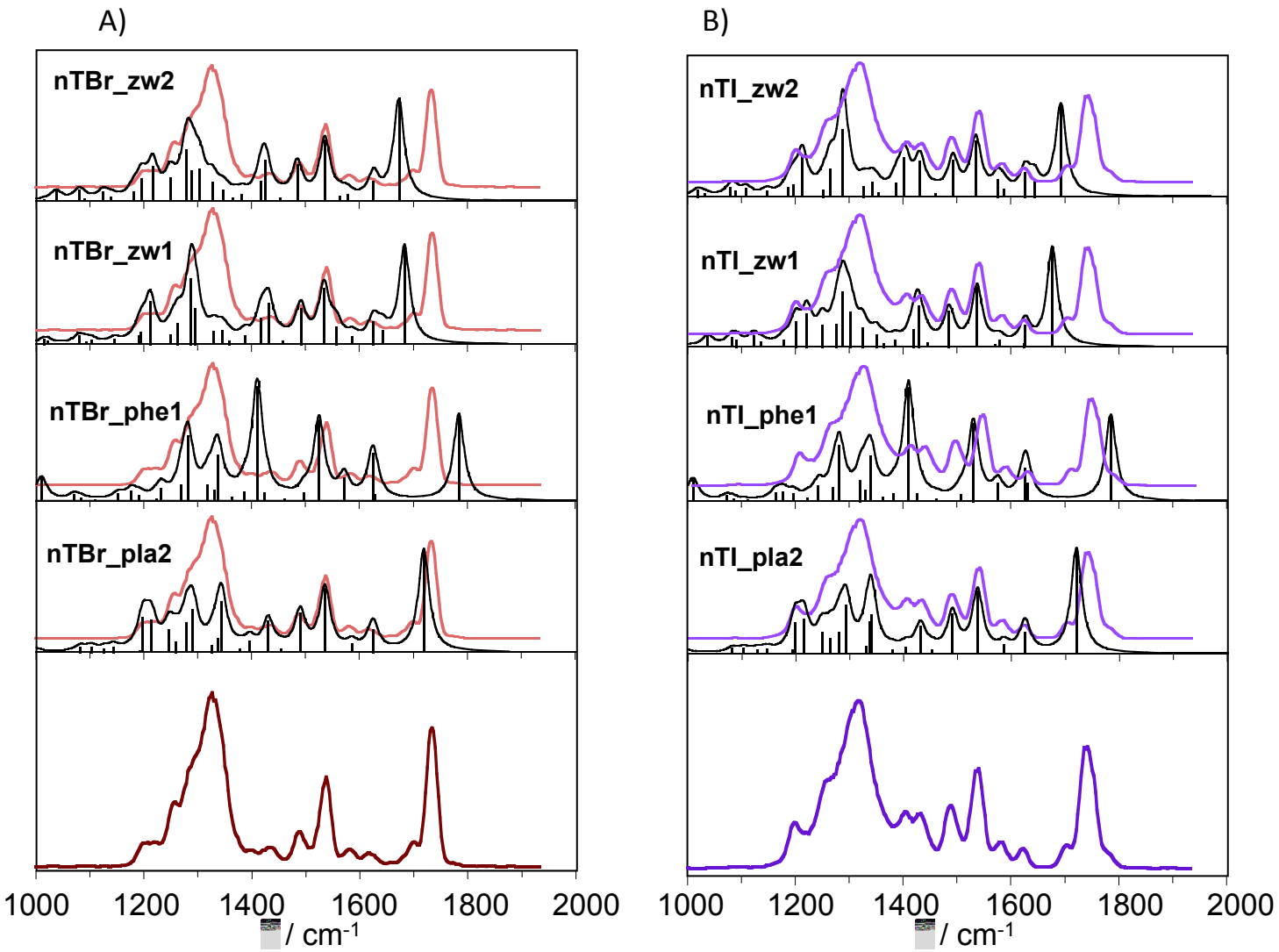

Fig. S18 Experimental IRMPD spectra of: $[nitroTyr+Br]^-$ (brown profile, panel A) compared with IR spectra [km mol^{-1}] for **nTBr_pla2**, **nTBr_phe1**, **nTBr_zw1** and **nTBr_zw2** structures; $[nitroTyr+I]^-$ (purple profile, panel B) compared with IR spectra [km mol^{-1}] for **nTI_pla2**, **nTI_phe1**, **nTI_zw1** and **nTI_zw2** structures. Theoretical vibrational modes were obtained at the B3LYP/6-311++G(d,p) level of theory and scaled by a factor of 0.978.

Table S1 Calculated energies (kJ mol^{-1}) at the B3LYP/6-311++G** level for the reaction: $[(nitro)Tyr+X]^- \rightarrow (nitro)Tyr + X^-$ (X = Cl, Br, I).

	[Tyr+X]$^-$		**[nitroTyr+X]$^-$**	
	ΔH_{298}	**ΔG_{298}**	**ΔH_{298}**	**ΔG_{298}**
X = Cl	121.21	96.01	153.01	124.08
X = Br	108.26	81.05	136.01	106.71
X = I	97.83	69.10	118.82	84.43

Table S2 Thermodynamic data (kJ mol^{-1}) for the most stable structures of [Tyr+X]$^-$ (X = Cl, Br, I) adducts calculated at different levels of theory.

	B3LYP[a]		B3LYP-D3[a]		MP2//B3LYP[b]	
	H_{rel}	**G_{rel}**	**H_{rel}**	**G_{rel}**	**H_{rel}**	**G_{rel}**
[Tyr+Cl]$^-$						
TCl_pla1	0.0	0.0	0.0	0.0	0.0	0.0
TCl_phe1	-4.8	-7.3	-3.2	-2.3	3.8	1.3
TCl_phe2	-5.3	-6.4	-0.7	-2.5	3.5	2.4
TCl_ter1	8.5	9.5	6.2	6.8	6.1	7.0
TCl_ter2	5.4	6.8	6.7	7.7	11.5	12.9
TCl_pla2	13.2	14.3	11.0	13.3	12.4	13.5
TCl_phe3	7.7	5.9	12.0	9.8	15.5	13.7
TCl_zw1	11.9	10.7	10.2	11.8	15.3	14.1
TCl_zw2	16.9	16.9	19.1	20.6	25.1	25.1
TCl_O1	79.3	80.6	78.3	78.2	83.8	85.0
[Tyr+Br]$^-$						
TBr_phe1	0.0	0.0	0.0	0.0	0.0	0.0
TBr_pla1	7.8	9.1	2.6	4.7	0.9	2.1
TBr_ter1	14.9	17.1	8.5	12.1	5.4	7.7
TBr_ter2	12.1	14.9	8.2	10.8	10.2	12.9
TBr_zw1	17.9	18.2	11.7	14.7	15.0	15.3
TBr_zw2	24.3	23.7	21.5	24.7	25.1	24.5
[Ty+-I]$^-$						
TI_phe1	0.0	0.0	0.0	0.0	0.0	0.0
TI_pla1	12.0	14.3	5.1	5.8	4.5	6.8
TI_ter1	15.3	17.9	9.7	11.3	9.4	12.1
TI_ter2	18.5	21.0	10.3	11.1	9.7	12.1
TI_zw1	20.3	24.1	13.2	16.6	14.6	18.4
TI_zw2	28.0	30.4	22.6	23.4	28.4	30.7

[a]The 6-311++G(d,p) basis set was employed. [b]Thermal and zero-point energy corrections obtained from B3LYP calculations. The Def2-TZVP ECP was used for iodine while keeping the 6-311++G(d,p) basis set for lighter atoms.

TABLE S3 Selected dihedral angles (in Degrees) of the lowest energy structures of $[Tyr+X]^-$ (X = Cl, Br, I) adducts, calculated at the B3LYP/6-311++G(d,p) level of theory.

	O1C1C2N	**NC2C3C1'**	**C2C3C1'C2'**	
Species	ϕ_1[a]	ϕ_2[b]	ϕ_3[c]	
[Tyr+Cl]⁻				
TCl_pla1	157.1	-67.3	102.4	gauche
TCl_phe1	10.2	-56.5	106.8	gauche
TCl_phe2	11.8	-59.5	98.0	gauche
TCl_ter1	-57.6	-176.7	82.3	anti
TCl_ter2	74.4	-163.8	93.9	anti
TCl_pla2	17.4	50.5	88.4	gauche
TCl_phe3	150.7	-58.7	97.8	gauche
TCl_zw1	19.4	51.2	79.8	gauche
TCl_zw2	1.4	-65.2	175.5	gauche
TCl_O1	54.8	-41.5	102.6	gauche
[Tyr+Br]⁻				
TBr_phe1	10.4	-57.2	107.2	gauche
TBr_pla1	155.3	-66.0	101.8	gauche
TBr_ter1	-57.3	-177.6	86.0	anti
TBr_ter2	74.6	-163.3	94.5	anti
TBr_zw1	17.6	50.9	77.5	gauche
TBr_zw2	0.1	-60.6	165.2	gauche
[Tyr+I]⁻				
TI_phe1	10.3	-55.9	109.2	gauche
TI_pla1	156.3	-60.8	103.5	gauche
TI_ter1	82.8	-168.7	86.1	anti
TI_ter2	-59.7	-175.2	87.3	anti
TI_zw1	15.6	53.1	76.6	gauche
TI_zw2	1.0	-67.0	-180.0	gauche

[a] ϕ_1 = O1C1C2N dihedral angle.
[b] ϕ_2 = NC2C3C1' dihedral angle.
[c] ϕ_3 = C2C3C1'C2' dihedral angle.

Table S4 Thermodynamic data (kJ mol^{-1}) for the most stable structures of [nitroTyr+X]$^-$ (X = Cl, Br, I) adducts calculated at different levels of theory.

	B3LYP[a]		B3LYP-D3[a]		MP2//B3LYP[b]	
	$\mathbf{H_{rel}}$	$\mathbf{G_{rel}}$	$\mathbf{H_{rel}}$	$\mathbf{G_{rel}}$	$\mathbf{H_{rel}}$	$\mathbf{G_{rel}}$
[nitroTyr+Cl]$^-$						
nTCl_pla1	0.0	0.0	0.0	0.0	0.0	0.0
nTCl_ter1	12.8	13.2	10.9	14.0	5.9	6.3
nTCl_pla2	12.6	13.4	11.4	12.3	10.5	11.3
nTCl_ring1	26.2	28.4	17.8	25.8	11.4	13.5
nTCl_ter2	19.1	20.2	18.4	19.9	15.7	16.8
nTCl_ter3	12.7	15.5	16.3	15.7	17.9	20.7
nTCl_pla3	20.6	23.4	18.5	23.3	18.6	21.4
nTCl_ter4	12.6	15.2	14.6	17.5	19.0	21.6
nTCl_phe1	32.6	29.0	38.0	34.4	26.7	23.1
nTCl_zw1	27.4	30.7	24.4	28.3	24.4	27.7
nTCl_zw2	23.6	23.6	24.6	27.0	28.3	28.3
nTCl_ring2	38.7	40.9	36.2	39.6	30.1	32.3
nTCl_O1	82.7	81.3	83.1	82.6	83.1	81.8
[nitroTyr+Br]$^-$						
nTBr_pla1	0.0	0.0	0.0	0.0	0.0	0.0
nTBr_ter1	12.3	13.3	10.9	13.1	8.4	9.3
nTBr_pla2	13.2	13.4	11.5	11.1	11.7	11.9
nTBr_ring1	25.6	26.7	19.9	21.7	10.8	12.0
nTBr_ter2	11.3	13.2	13.4	13.6	17.3	19.3
nTBr_phe1	32.2	28.6	38.0	33.4	27.5	23.9
nTBr_zw1	27.1	29.9	24.8	27.6	24.0	26.7
nTBr_zw2	22.6	21.9	21.4	24.9	28.0	27.3
[nitroTyr+I]$^-$						
nTI_pla1	0.0	0.0	0.0	0.0	0.0	0.0
nTI_ter1	10.4	7.3	9.6	9.5	10.2	7.1
nTI_pla2	13.5	12.6	11.5	10.9	9.7	8.8
nTI_ring1	24.8	21.7	13.8	15.3	17.0	13.8
nTI_ter2	10.0	11.0	12.9	13.4	15.0	15.9
nTI_phe1	29.6	24.2	36.2	31.4	23.4	18.0
nTI_zw1	21.5	19.9	23.4	23.4	22.1	20.4
nTI_zw2	25.6	26.7	23.9	26.0	20.3	21.5

[a]The basis set 6-311++G(d,p) was employed. [b]Thermal and zero-point energy corrections obtained from B3LYP calculations. The Def2-TZVP ECP was used for the iodine atom together with the 6-311++G(d,p) basis set for lighter atoms.

TABLE S5 Selected dihedral angles (in Degrees) of the lowest energy structures of [nitroTyr+X]$^-$ (X = Cl, Br, I) adducts, calculated at the B3LYP/6-311++G(d,p) level of theory.

	O1C1C2N	**NC2C3C1'**	**C2C3C1'C2'**	
Species	ϕ_1 [a]	ϕ_2 [b]	ϕ_3 [c]	
[nitroTyr+Cl]$^-$				
nTCl_pla1	159.1	-66.0	101.2	gauche
nTCl_ter1	-56.3	-178.3	96.6	anti
nTCl_pla2	162.5	-62.9	81.5	gauche
nTCl_ring1	-25.3	62.6	84.6	gauche
nTCl_ter2	-55.2	-175.8	69.8	anti
nTCl_ter3	74.9	-166.8	67.4	anti
nTCl_pla3	9.9	-59.5	109.7	gauche
nTCl_ter4	73.4	-163.5	99.4	anti
nTCl_phe1	9.4	-60.0	104.8	gauche
nTCl_zw1	18.7	48.9	92.5	gauche
nTCl_zw2	15.0	61.1	70.1	gauche
nTCl_ring2	9.9	-59.5	109.7	gauche
nTCl_O1	52.5	-50.1	99.0	gauche
[nitroTyr+Br]$^-$				
nTBr_pla1	157.9	-63.7	102.4	gauche
nTBr_ter1	-55.6	-179.7	94.7	anti
nTBr_pla2	161.2	-61.2	79.7	gauche
nTBr_ring1	106.1	62.4	83.1	gauche
nTBr_ter2	74.6	-165.0	98.2	anti
nTBr_phe1	9.6	-60.2	105.1	gauche
nTBr_zw1	-10.4	65.6	86.3	gauche
nTBr_zw2	14.2	59.8	71.3	gauche
[nitroTyr+I]$^-$				
nTI_pla1	158.1	-59.9	103.0	gauche
nTI_ter1	-54.0	-177.8	84.1	anti
nTI_pla2	159.3	-60.6	77.5	gauche
nTI_ring1	-13.6	61.9	81.5	gauche
nTI_ter2	77.6	-164.2	102.7	anti
nTI_phe1	14.1	59.4	72.3	gauche
nTI_zw1	10.1	-60.1	106.2	gauche
nTI_zw2	-8.6	65.6	85.69	gauche

[a] ϕ_1 = ∠O1C1C2N dihedral angle.
[b] ϕ_2 = ∠NC2C3C1' dihedral angle.
[c] ϕ_3 = ∠C2C3C1'C2' dihedral angle.

Table S6 Experimental IRMPD resonances and calculated (at B3LYP/6-311++G(d,p) level of theory) vibrational frequencies for the low-lying isomers of $[Tyr+X]^-$ (X = Cl, Br, I) adducts.

$[Tyr+Cl]^-$					
IRMPD[a]	Calculated[a,b]				Vibrational mode
	TCl_pla1	**TCl_phe1**	**TCl_ter1**	**TCl_ter2**	
1105 (low)	1104 (20)		1083 (32)	1097 (53)	NH2 wagging
1178				1168 (112)	CH in plane bend
	1166 (176)		1168 (172)	1171 (77)	OH phenol bend
	1194 (47)	1178 (33)		1197 (66)	OH carboxyl bend + NH2 wagging
1250		1250 (37)		1223 (57)	OH phenol bend
	1230 (64)		1232 (90)	1233 (80)	ring def
	1270 (21)				NH2 twist
1312		1293 (238)	1307 (45)		ring def
1358	1336 (22)				CH in plane bend
	1352 (293)		1329 (159)	1337 (96)	OH carboxyl bend
			1334 (138)		OH carboxyl bend+OH phenol bend
				1365 (168)	COO-H bend + NH2 twisting
1376		1378 (32)			OH phenol bend
	1395 (60)		1355 (46)	1379 (102)	CH bend
		1397 (474)			OH carboxyl bend
1451 (shoulder)		1447 (46)			OH phenol bend
1507	1507 (132)	1509 (185)	1507 (113)	1506 (120)	CH in plane bend
1608	1615 (26)	1610 (190)	1626 (26)	1615 (29)	ring def
	1633 (35)	1627 (22)			NH2 scissor
1720	1713 (442)		1714 (364)	1706 (368)	C=O stretch
1790		1781 (389)			C=O stretch
	2710 (1871)		2850 (1705)	2759 (1879)	OH carboxyl stretch
		2751 (2962)			OH phenol stretch
			2918 (38)		CH stretch
	2898 (32)	2884 (29)			CH2 symm stretch
	2994 (44)	2998 (21)		2994 (32)	CH asymm stretch
3008	3004 (42)		3005 (29)		CH symm stretch
3060	3046 (21)	3037 (32)			CH symm stretch
3200 (broad)		3242 (343)			OH carboxyl stretch
3272			3239 (218)	3242 (209)	NH2 symm stretch
3330			3381 (20)	3368 (25)	NH2 asymm stretch
3663	3676 (45)		3680 (48)	3671 (47)	OH phenol stretch

$[Tyr+Br]^-$					
IRMPD[a]	Calculated[a,b]				Vibrational mode
	TBr_phe1	**TBr_pla1**	**TBr_ter1**	**TBr_ter2**	
1104 (low)		1103 (20)	1081 (29)	1096 (50)	NH2 wag

1177		1166 (173)	1168 (183)	1168 (192)	OH phenol bend
	1170 (26)				CH in plane bend
	1179 (28)				OH carboxyl bend + NH2 wagging
1204		1189 (66)		1191 (70)	CH bend
1242	1243 (60)				OH phenol bend
		1232 (63)	1233 (91)	1233 (85)	ring def
1295	1287 (224)				ring def
1333		1328 (42)	1307 (63)	1299 (62)	OH carboxyl bend + CH2 wagging
		1337 (33)		1331 (34)	OH phenol bend + CH in plane bend
		1341 (268)	1328 (243)	1324 (148)	OH carboxyl bend
			1333 (45)		OH phenol bend + CH in plane bend
1375 (shoulder)				1357 (127)	OH carboxyl bend + CH bend
	1367 (26)				OH phenol bend + CH in plane bend
		1396 (41)	1358 (32)	1378 (46)	CH bend
	1397 (476)				OH carboxyl bend
1447 (low)	1442 (33)				OH phenol bend + ring def
1508	1511 (180)	1508 (127)	1507 (116)	1506 (120)	CH in plane bend
1602	1611 (178)	1615 (28)	1616 (27)	1615 (30)	ring def
1729		1718 (439)	1719 (371)	1712 (372)	C=O stretch
1775	1781 (388)				C=O stretch
2841	2880 (42)	2892 (26)	2898 (22)	2906 (25)	CH2 symm stretch
2921	2929 (2685)				OH phenol stretch
			2913 (36)	2922 (352)	CH stretch
			2942 (25)		CH2 asymm stretch
		2904 (1784)	2976 (1663)	2930 (1538)	OH carboxyl stretch
		2931 (47)			CH stretch
3022 (broad)	2994 (27)	2992 (47)	3000 (27)	2994 (30)	CH asymm stretch
	3033 (67)	3002 (39)			CH symm stretch
		3040 (21)			CH symm stretch
3251 (broad)	3236 (345)				OH carboxyl stretch
			3238 (240)	3245 (242)	NH2 symm stretch
3331		3314 (5)			NH2 symm stretch
3400	3412 (10)	3392 (7)	3378 (20)	3371 (27)	NH2 asymm stretch
3664		3667 (46)	3672 (48)	3670 (48)	OH phenol stretch

[Tyr+I]$^-$					
IRMPD[a]	Calculated[a,b]				Vibrational mode
	TI_phe1	**TI_pla1**	**TI_ter1**	**TI_ter2**	
1090 (low)		1092 (20)	1078 (26)	1089 (38)	NH2 wag + CH in plane bend
1177	1171 (24)			1166 (71)	CH in plane bend
		1166 (164)	1168 (189)	1170 (114)	OH bend
	1181 (38)				OH carboxyl bend + NH2 wagging
		1189 (78)		1183 (101)	CH bend
1239 (shoulder)			1223 (77)		OH carboxyl bend + NH2 wagging
	1228 (80)				OH phenol bend
		1231 (79)	1234 (79)	1234 (91)	ring def
1288			1289 (256)		OH carboxyl bend + CH in plane bend
	1284 (210)				ring def
1323	1353 (29)				OH phenol bend + CH in plane bend

		1320 (34)	1314 (51)	1329 (45)	OH carboxyl bend + CH in plane bend
		1328 (257)		1333 (120)	OH carboxyl bend
		1339 (44)			CH2 wag
			1356 (26)	1365 (141)	CH bend
1382	1399 (479)				OH carboxyl bend
		1400 (33)		1381 (35)	NH2 twist
1517	1513 (175)	1507 (120)	1508 (119)	1504 (116)	CH in plane bend
1608	1613 (160)	1614 (33)	1616 (28)	1614 (33)	ring def
		1632 (35)			NH2 scissor
1750		1728 (440)	1731 (375)	1724 (368)	C=O stretch
1785	1783 (386)				C=O stretch

[a] In cm^{-1}. [b] The reported intensities given in parentheses are in km mol^{-1}. Bands with an intensity lower than 20 km mol^{-1} are usually not included. Frequencies are scaled by a factor of 0.978 in the 1000-2000 cm^{-1} region and 0.955 in the 2800-3800 cm^{-1} region.

Table S7 Experimental IRMPD resonances and calculated (at B3LYP/6-311++G(d,p) level of theory) vibrational frequencies for the low-lying isomers of [nitroTyr+X]$^-$ (X = Cl, Br, I) adducts.

[nitroTyr+Cl]$^-$

IRMPD[a]	Calculated[a,b] **nTCl_pla1**	**nTCl_ter1**	**nTCl_ring1**	Vibrational mode
			1001 (43)	NH2 wag
	1083 (25)	1079 (42)	1079 (28)	ring def + NO2 symm stretch
	1147 (37)	1133 (24)	1134 (40)	CH in plane bend + NH2 twist
1220	1191 (73)	1191 (64)	1197 (47)	CH in plane bend + OH phenol bend
	1207 (305)	1211 (247)	1216 (197)	C-N stretch + CH in plane bend
1330		1247 (33)	1241 (27)	OH carboxyl bend
	1252 (140)	1253 (113)	1249 (125)	OH phenol bend + CH in plane bend + NO2 symm stretch
			1281 (132)	CH bend
	1280 (341)	1284 (302)	1291 (237)	OH phenol bend
	1294 (29)	1313 (33)		CH2 twist
	1341 (100)			ring def
	1357 (218)	1324 (271)	1316 (250)	OH carboxyl bend
		1339 (55)	1337 (128)	OH carboxyl bend + CH2 twist
		1344 (135)		CH2 wag
	1392 (73)			NH2 twist
1423	1422 (184)	1422 (159)	1426 (165)	NO2 asymm stretch + OH phenol bend
1474	1482 (172)	1485 (140)	1487 (116)	NO2 asymm stretch + CH in plane bend
1528	1530 (271)	1531 (273)	1533 (245)	NO2 asymm stretch + ring def
1572			1584 (41)	ring def
1610	1625 (76)	1627 (74)	1630 (59)	ring def
1710	1720 (448)	1715 (360)	1698 (415)	C=O stretch

[nitroTyr+Br]$^-$

IRMPD[a]	Calculated[a,b] **nTBr_pla1**	**nTBr_ter1**	**nTBr_ring1**	Vibrational mode
	1083 (26)	1079 (43)	1079 (28)	ring def + NO2 sym stretch
	1147 (40)	1133 (24)	1134 (41)	CH in plane bend + NH2 twist
1197	1188 (31)		1163 (29)	CH bend
	1193 (55)	1191 (65)	1192 (31)	CH in plane bend + OH phenol bend
		1204 (82)		CH2 wag + NH2 twist
1214	1208 (293)	1211 (169)	1213 (210)	C-N stretch + CH in plane bend

1257		1240 (27)	1228 (39)	OH carboxyl bend
	1252 (120)	1253 (126)	1250 (133)	OH phenol bend + CH in plane bend + NO2 symm stretch
			1282 (151)	CH bend + CH2 twist
	1279 (295)	1284 (297)		OH phenol bend
	1292 (72)		1292 (223)	CH2 twist
1323	1326 (47)			CH2 wag
	1337 (107)	1314 (315)	1307 (237)	OH carboxyl bend
		1318 (55)		OH carboxyl bend + CH2 wag
	1340 (214)	1347 (109)	1337 (110)	OH carboxyl bend + CH2 twist
	1394 (46)			NH2 twist
1437	1422 (180)	1422 (156)	1426 (159)	NO2 asym stretch + OH phenol bend
1487	1484 (166)	1484 (147)	1487 (115)	NO2 asym stretch + CH in plane bend
1538	1531 (267)	1531 (270)	1534 (242)	NO2 asym stretch + ring def
1579	1581 (44)	1581 (38)	1583 (39)	ring def
1618	1625 (83)	1627 (76)	1630 (58)	ring def
	1630 (31)		1638 (66)	NH2 scissor
1698			1705 (414)	C=O stretch
1733	1726 (450)	1720 (365)		C=O stretch

[nitroTyr+I]$^-$

IRMPD[a]	Calculated[a,b]			Vibrational mode
	nTI_pla1	**nTI_ter1**	**nTI_ring1**	
	1083 (27)	1078 (39)	1077 (29)	ring def + NO2 symm stretch
			1133 (38)	CH in plane bend
	1147 (43)		1159 (23)	CH in plane bend + NH2 twist
1198	1187 (45)			CH bend
		1187 (45)	1195 (33)	OH carboxyl bend
	1195 (46)	1193 (49)		CH in plane bend + OH phenol bend
	1211 (294)	1213 (229)	1215 (179)	C-N stretch + CH in plane bend
1253		1221 (54)		OH carboxyl bend + NH2 twist
	1251 (124)	1252 (145)	1251 (133)	OH phenol bend + CH in plane bend + NO2 symm stretch
			1281 (64)	CH bend + CH2 twist
	1285 (345)	1283 (155)	1291 (300)	OH phenol bend
1316	1300 (30)			CH2 twist
		1291 (480)	1300 (308)	OH carboxyl bend
	1326 (265)			OH carboxyl bend + CH2 wag

	1335 (30)		1337 (103)	OH carboxyl bend + CH2 twist
	1343 (80)	1341 (114)		CH2 wag
			1381 (22)	OH phenol bend + ring def
1403	1397 (33)			NH2 twist
1431	1424 (187)	1423 (146)	1426 (144)	NO2 asymm stretch + OH phenol bend
1488	1484 (167)	1485 (151)	1487 (117)	NO2 asymm stretch + CH in plane bend
1540	1530 (254)	1532 (264)	1536 (241)	NO2 asymm stretch + ring def
1580	1581 (50)	1581 (37)	1581 (36)	ring def
1621	1626 (88)	1628 (83)	1631 (108)	ring def
	1633 (33)		1624 (62)	NH2 scissor
1705			1716 (383)	C=O stretch
1743	1733 (439)	1729 (364)		C=O stretch

[a] In cm^{-1}. [b] The reported intensities given in parentheses are in km mol^{-1}. Bands with an intensity lower than 20 km mol^{-1} are not included. Frequencies are scaled by a factor of 0.978.